Anal Bioanal Chem (2015) 407:7467–7475
DOI 10.1007/s00216-015-8913-x

RESEARCH PAPER

A guiding light: spectroscopy on digital microfluidic devices using in-plane optical fibre waveguides

Kihwan Choi[1,3,4] · **Jared M. Mudrik**[1] · **Aaron R. Wheeler**[1,2,3]

Received: 9 April 2015 / Revised: 24 June 2015 / Accepted: 13 July 2015 / Published online: 2 August 2015

Abstract We present a novel method for in-plane digital microfluidic spectroscopy. In this technique, a custom manifold (.stl file available online as ESM) aligns optical fibres with a digital microfluidic device, allowing optical measurements to be made in the plane of the device. Because of the greater width vs thickness of a droplet on-device, the in-plane alignment of this technique allows it to outperform the sensitivity of vertical absorbance measurements on digital microfluidic (DMF) devices by ~14×. The new system also has greater calibration sensitivity for thymol blue measurements than the popular NanoDrop system by ~2.5×. The improvements in absorbance sensitivity result from increased path length, as well as from additional effects likely caused by liquid lensing, in which the presence of a water droplet between optical fibres increases fibre-to-fibre transmission of light by ~2× through refraction and internal reflection. For interrogation of dilute samples, stretching of droplets using digital microfluidic electrodes and adjustment of fibre-to-fibre gap width allows absorbance path length to be changed on-demand. We anticipate this new digital microfluidic optical fibre absorbance and fluorescence measurement system will be useful for a wide variety of analytical applications involving microvolume samples with digital microfluidics.

Keywords Digital microfluidics · Microfluidics · Fluorescence · Absorbance · Spectrophotometry · UV/Vis · Fibre optics · Optical fibres · Waveguides

Kihwan Choi and Jared M. Mudrik contributed equally to this work.

Electronic supplementary material The online version of this article (doi:10.1007/s00216-015-8913-x) contains supplementary material, which is available to authorized users.

✉ Aaron R. Wheeler
aaron.wheeler@utoronto.ca

[1] Department of Chemistry, University of Toronto, 80 St. George Street, Toronto, Ontario M5S 3H6, Canada

[2] Institute of Biomaterials and Biomedical Engineering, University of Toronto, 164 College Street, Toronto, Ontario M5S 3G9, Canada

[3] Donnelly Centre for Cellular and Biomolecular Research, 160 College Street, Toronto, Ontario M5S 3E1, Canada

[4] Present address: Division of Metrology for Quality of Life, Korea Research Institute of Standards and Science, Yuseong-gu, Daejeon 305-340, Korea

Introduction

Small samples are a reality of modern chemical analyses. From biological specimens to forensic evidence, the need to efficiently handle and measure small volumes of liquid is ever present. Several techniques have been developed for the analysis of small samples, including microwell plate readers [1], microscope spectrometers [2], microspectrometers [3] and microchannels [4]. In the case of microchannel-based microfluidics, optical detection has proven popular because of the small instrumentation footprint and ease of integration with devices [5]. Several innovations have further enhanced the utility of optical detection in microchannels, including device-integrated reflectors [4, 6], filters [7], attenuators [8], waveguides [9, 10] and microlenses [11, 12]. The integration of optofluidic technologies with microchannels has paved the way for the development of a variety of optical lab-on-a-chip systems, such as cell sorting [13], microscopy [14], particle analysis [15], surface-enhanced Raman spectroscopy [16] and cavity ring-down spectroscopy [17].

Digital microfluidics (DMF) is an alternative to microchannels for microscale fluid handling that facilitates the manipulation of nanolitre- to microlitre-volume

droplets over an array of dielectric-coated electrodes [18, 19]. Through electrodynamic forces, liquid droplets are individually actuated in two dimensions over these electrodes, which enables precise control over sample processing and reactions. (Note that related techniques in which stationary droplet shapes are electrically modulated to facilitate lensing or reflection effects [20–22] are quite interesting and useful, but they are not capable of implementing reactions and sample processing and are thus not typically known as "DMF".) Traditionally, optical analysis of DMF samples has been performed perpendicularly in the "*z*" dimension [23–25]. However, since DMF devices are typically quite thin (on the order of hundreds of microns), measuring perpendicularly results in a short path length and poor sensitivity (particularly for absorbance spectroscopy). This shortcoming can be remedied by measuring through the (relatively greater) width of a droplet in the plane of the device.

There are two potential geometries for in-plane interactions between optics and droplets in DMF systems. In the first geometry [26, 27], droplets are manipulated along the side of an optical fibre, changing the reflectivity and thus modulating the light transmission through the fibre. This geometry is particularly useful for forming DMF-enabled optical attenuators but has not been used (to our knowledge) in a scheme that solves the problem of poor sensitivity for absorbance measurements. In the second geometry, droplets are moved between two fibres, one serving as the light source and one as collector. The one example of this format that we are aware of was described by Ceyssens et al. [28], who integrated microfabricated epoxy waveguides on a DMF device. This was an important first step and inspired the work described here but suffers from a few limitations, including (a) the epoxy material suffers from poor transmission relative to traditional glass optical fibres, (b) the epoxy waveguides are permanent—once formed, they cannot be moved (thus blocking a portion of the array from being useful for droplet movement) and (c) the interface is operated with the droplet contacting the fibres, raising concerns about sample carry-over (in terms of adsorption to the fibres) between experiments.

We present a new method for in-plane UV/Vis absorbance and fluorescence spectroscopy with fused silica optical fibre waveguides on a DMF platform. The fibres are aligned in the plane of a DMF device, allowing contact-free optical measurements through the width of a droplet. A custom manifold allows insertion and alignment of fibres in seconds, permitting rapid adjustment of path length between fibres for trace analysis and variable dynamic range measurements. We anticipate the integration of optical fibre waveguides with DMF will be of use for on-chip chemical and biochemical analyses incorporating optical detection.

Experimental

Reagents and materials

Unless otherwise specified, general use reagents were purchased from Sigma Chemical (Oakville, ON, Canada). Thymol blue was obtained from Bioshop (Burlington, ON, Canada). Stable peroxide substrate buffer and 3,3′,5,5′-tetramethylbenzidine (TMB) substrate were purchased from Thermo Scientific (Rockford, IL). Pluronic L64 (BASF Corp., Germany) was generously donated by Brenntag Canada (Toronto, ON, Canada). Parylene-C dimer was from Specialty Coating Systems (Indianapolis, IN), and Teflon AF was purchased from DuPont (Wilmington, DE). Deionised (DI) water had a resistivity of 18 MΩ cm at 25 °C.

A 20 mM phosphate buffer was prepared by mixing Na_2HPO_4 and NaH_2PO_4 solutions, and the pH was adjusted to 6.0. A 20 mM tetraborate buffer was prepared in DI water, and the pH was adjusted to 10.0 by titrating with 0.1 M NaOH solution. Fluorescein stock solution (5 mM) was prepared in 20 mM tetraborate buffer. Horseradish peroxidase solution formed by dissolving horseradish peroxidase (HRP) in phosphate-buffered saline solution (0, 50, 100, 200 and 500 μU/mL supplemented with 0.05 % *v*/*v* Pluronic L64). Stop solution was adapted from TSH well plate ELISA kits from Calbiotech (Spring Valley, CA). All solutions were supplemented with Pluronic L64 (0.04 % *v*/*v*) prior to use.

DMF device fabrication and operation

Digital microfluidic devices were fabricated in the Toronto Nanofabrication Center (TNFC) clean room facility as described previously [29]. Briefly, chromium and photoresist (AZ1500) coated glass substrates (Telic Co., Valencia, CA) were patterned through photolithography and wet etching with a transparent photomask (Pacific Arts and Design, Markham, ON, Canada). Then, DMF bottom plates were coated with ~7 μm of Parylene-C and ~200 nm of Teflon AF. The top plates of DMF devices were prepared by coating Teflon AF (~200 nm) on unpatterned indium-tin oxide-coated glass slides (Delta Technologies Ltd, Stillwater, MN).

The bottom plate on most devices featured an array of 96 actuation electrodes (2.2×2.2 mm each) connected to ten reservoir electrodes (4.5×4.5 mm each). The bottom plate on other devices featured the same geometry of electrodes but with a series of 4.5-mm-diameter circular apertures (free from metal) formed at the intersection of two electrodes (as described previously [30]) to facilitate *z*-dimension optical measurements. Each top plate was joined with a bottom plate via a 270-μm-thick spacer, resulting in a unit droplet (i.e. a droplet that covers one actuation electrode) of ~2-mm diameter with 1.2 μL. To drive droplet movement, AC potentials (~150 V_{RMS}, 10 kHz) were applied to the electrodes with a function

generator (Agilent Technologies, Santa Clara, CA) and a high-voltage amplifier (TREK Inc., Medina, NY).

DMF optical fibre interface

A 120 mm×100 mm×12-mm manifold designed to interface optical fibres and DMF devices was formed by a commercial 3D printing company (3D Prototype Design, New Hamburg, ON). The .stl file for the design is included in the Electronic Supplementary Material (ESM). The manifold features a hollow bay matching the dimensions of a DMF device surrounded by walls bearing twelve 5-mm-diameter through-holes (three holes in each wall). Fingertight fittings (IDEX Health & Science, Oak Harbor, WA) were fixed in the holes to align optical fibres jacketed with 0.010-in. i.d. PEEK sleeves (IDEX Health & Science).

As shown in Fig. 1, in each experiment, a DMF device was placed in the manifold, and two 240-μm o.d., 200-μm core diameter, 0.22 numerical aperture optical fibres (Thorlabs, Newton, NJ) were inserted into the manifold and between the two plates of the DMF device from opposite sides. The gap between the two fibres was approximately 4 mm for unit droplet measurements and was extended to ~6 or ~8 mm, for two- and three-unit volumes, respectively. A Xenon lamp (PX-2, Ocean Optics, Dunedin, FL) and a spectrometer (USB4000, Ocean Optics) were connected to the ends of the two fibres, respectively. Data were collected using SpectraSuite software (Ocean Optics).

On-chip serial dilution and absorbance analysis of thymol blue

Serial dilutions of thymol blue were formed on-chip and analysed in an iterative process. In step 1, one unit droplet of 100 μM thymol blue in 20 mM tetraborate buffer (pH 10.1) was dispensed from a reservoir and driven to the gap between the source and collection fibres. In step 2, wavelength-resolved light intensities were recorded (180 to 890 nm with an integration time of 300 ms, averaged over five spectra). In step 3, one unit droplet of diluent (20 mM tetraborate buffer, pH 10.1) was dispensed from a reservoir and merged with the thymol blue droplet and then actively mixed by actuating the pooled droplet in a circular motion across four electrodes for 1 min. In step 4, the pooled droplet was split into two unit droplets—one droplet for the next dilution and the other droplet for measurement. In step 5, the measurement-droplet (one unit volume) was delivered to the detection region and evaluated spectroscopically as above. In step 6, the measurement-droplet was moved to the waste reservoir. Steps 3–6 were then repeated (using the droplet saved from the previous iteration) three times to generate and analyse the dilution series (representing a total of 18 discrete steps). Prior to forming and measuring each dilution series, a blank measurement of a unit droplet of 20 mM tetraborate buffer (pH 10.1) was collected using the same parameters above to estimate absorbance A according to Eq. (1)

$$A = \log\left(I_{\text{blank}}/I_{\text{analyte}}\right) \quad (1)$$

where I_{blank} and I_{analyte} are the intensities of the analyte and the blank at each wavelength. For quantitative analysis, absorbance values at 600 nm were averaged, plotted as a function of concentration and fitted with linear regression analysis.

For z-axis measurements, a similar protocol to the one described above was used, except that (a) devices with a transparent aperture in the bottom plate (see above) were used, and (b) the measurement-droplets had quadruple-unit volume (3.2 μL) to ensure that each droplet covered the entire aperture. For each measurement, after formation of the appropriate dilution and delivery of the measurement-droplets to the

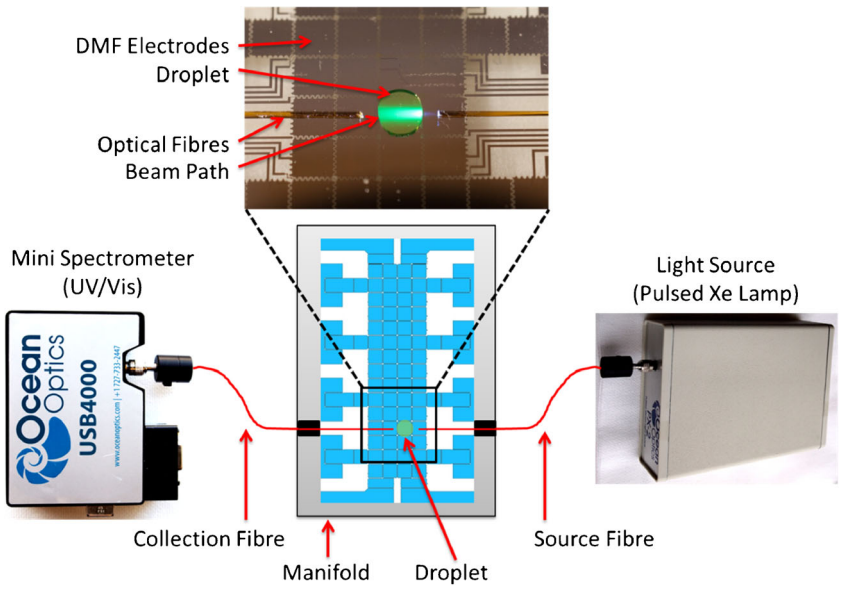

Fig. 1 Photo (*top*) and schematic (*bottom*) of a DMF device interfaced via a custom 3D-printed manifold (see the .stl file in the ESM) and optical fibres to a light source and a spectrometer. In the photo, the droplet contains fluorescein (100 μM) to make the light beam visible. The optical fibres are held in alignment by the manifold

aperture, the device was affixed with tape to an empty 96-well Stripwell plate and inserted into a Sunrise microplate reader (Tecan, Durham, NC). Measurements at 600 nm were collected in 'accuracy mode', and absorbance values (Eq. 1) were averaged, plotted as a function of concentration and fitted with linear regression analysis.

Off-chip thymol blue absorbance measurements

Solutions containing 3, 6, 12.5, 25, 50 and 100 μM of thymol blue were prepared in 20 mM borate buffer (pH 10.1) by manual pipetting. For each measurement, a 2-μL aliquot of solvent (20 mM borate buffer solution) was pipetted onto the pedestal of a NanoDrop 1000 (Thermo Fisher Scientific, Wilmington, DE), and a reference spectrum of signal intensities from 220 to 750 nm was obtained with the 'UV/VIS Absorbance' module. This process was then repeated with thymol blue solutions; between each measurement, the surface of the pedestal was cleaned with a lint-free tissue (Kimwipe, Kimberly Clark, Roswell, Ga). Absorbance values at 600 nm (Eq. 1) were averaged, plotted as a function of concentration and fitted with linear regression analysis.

On-chip fluorescence and absorbance measurements of fluorescein

An aliquot of 100 μM fluorescein in 20 mM borate buffer (pH 10.1) was loaded into a reservoir. One unit droplet was dispensed from the reservoir and moved to the 4-mm gap between optical fibres. A 'white' LED flashlight (Sipik SK68, China) was positioned 8 cm above the DMF device to illuminate the droplet. Absorbance (with Xe lamp on and LED off) and emission (with Xe lamp off and LED on) spectra were measured with the spectrometer (using the parameters outlined above) and evaluated using SpectraSuite software (Ocean Optics). Stray light from the LED flashlight was subtracted from fluorescence spectra through blank correction in the SpectraSuite software.

Liquid lens effect

The transmission intensity between source and collection optical fibres (4-mm gap) was measured with air and with a unit droplet of DI water in the gap. The resulting transmission intensity was averaged over the range of 250–800 nm. Ray tracing simulations were performed using TracePro software (Lambda Research Corporation, Littleton, MA) on a model in which source and collection optical fibres (200-μm core diameter, 4-mm gap between the two fibres) resided between simulated DMF top and bottom plates, simulated as a layer of Teflon AF (7 μm, refractive index 1.305) and as a layer of Teflon AF (7 μm) over a layer of chromium (modelled as a perfect reflector), respectively. In one model, the gap between the two fibres was filled with air (refractive index = 1.00), and in the other model, a cylindrical water droplet (2-mm diameter, refractive index = 1.33) was centred in the gap, sandwiched between the top and bottom plates. Ray tracing simulations (1×10^5 rays) were performed on the models, and the resulting light intensities reaching the collection fibre were compared. The ray source (end of source fibre) was set up as a circular grid (rays originating from 100 concentric rings, grid normal to vector of source fibre) with uniform spatial distribution and Gaussian angular distribution (chosen as simplifying assumptions), with rays emitted in a cone with half angle 12.7°.

On-chip absorbance measurements of fluorescein with varying path length

For the absorbance measurements of droplets with greater than unit droplet volume, the gap between the two fibres was adjusted manually before actuating the droplets. In each measurement, an analyte solution (10 μM fluorescein in 20 mM borate) was loaded into a reservoir, and one, two or three unit volume droplets were dispensed. The droplets were merged (when more than one) and then actuated to the 4-, 6-, or 8-mm gap between fibres to collect absorbance spectra using the parameters described above. During each measurement, AC potentials were applied to the one, two or three electrodes centred between the fibres to maintain the stretched droplet shape. Each measurement was accompanied by blank measurements (of 20 mM borate) using the same procedure, and absorbance values at 488 nm (Eq. 1) were used to compare the different signals.

On-chip enzymatic colorimetric assay of TMB

In each experiment, aliquots of HRP standard solution (at one of five concentrations, see above), H_2O_2, TMB and stop solution were loaded into different reservoirs. One unit droplet each of HRP, H_2O_2 and TMB were dispensed, merged and actively mixed. After the pooled droplet was incubated for 5 min, one unit droplet of stop solution was dispensed and driven to the pooled droplet and mixed for 1 min. Then, one unit droplet was split from the pooled droplet and moved to the 4-mm gap between the optical fibres. An optical intensity spectrum was measured using the parameters above for each concentration of HRP (including a blank with 0 mM HRP). Absorbance values (Eq. 1) at 450 nm were averaged, plotted as a function of concentration and fitted with linear regression analysis. The limit of detection was defined as the concentration corresponding to the average signal of the blank plus three standard deviations of the blank signal measurement.

On-chip solid-phase extraction and fluorescence measurement

Porous polymer monolith (PPM) discs with C12 functionality were prepared and integrated onto DMF devices as described previously [31]. A five-step process was developed to implement on-chip SPE. First, a PPM disc on one side of a DMF device was activated by dispensing and driving a 3-μL droplet of acetonitrile onto the disc where it was incubated for 1 min. Second, the PPM was rinsed by dispensing and driving a 3-μL droplet of 0.5 % aqueous formic acid onto and off of the disc. Third, a 9-μL droplet of fluorescein (30 μM in 0.5 % formic acid) was dispensed, driven onto the PPM and incubated with active mixing for 5 min. Fourth, the sample droplet was driven away, and the PPM was rinsed by dispensing and driving two 3-μL droplets of 0.5 % aqueous formic acid onto and off of the disc. Fifth, the sample was eluted by dispensing and driving a 3-μL droplet of borate buffer (500 mM, pH 9) onto and off of the disc. After elution, the eluate droplet was actuated to the other side of the DMF device, where it was interrogated for fluorescence using the DMF optical fibre setup for emission measurement, using a perpendicularly aligned diode laser (405 nm, 5 mW, DealExtreme, China) for excitation. Fluorescence emission intensities at 521 nm were collected in triplicate and processed using SpectraSuite software.

To evaluate the eluate concentrations, a calibration curve was constructed from fluorescein standards prepared off-chip in borate buffer (500 mM, pH 9). A 3-μL droplet of each standard concentration was loaded onto the DMF device and measured in triplicate using the optical fibre system, as described above. Calibration data were averaged, plotted as a function of concentration and fitted with linear regression analysis.

Results and discussion

An in-plane optical fibre interface for DMF

The vast majority of digital microfluidic applications interfaced with absorbance detection described previously (e.g. optical density measurements of microorganism growth rates [23], enzymatic colorimetric assays for glucose concentration [24] and real-time concentration monitoring for liquid microextractions [25]) have been designed such that signals are collected at a perpendicular "*z*"-axis relative to the plane of the device (with one exception [28]). The optical path length in perpendicular measurements is very short (e.g. in the devices reported here, the *z*-dimension path length is 270 μm), which limits the sensitivity according to the Lambert-Beer law. Borrowing from similar techniques developed for microchannel devices [4, 32], we hypothesised that an in-plane detection system would be useful for improving path length (and thus sensitivity) in optical measurements. In such a system, the droplet width, which is often much larger (e.g. in the devices reported here, unit volume droplets are ~2-mm diameter), defines the path length.

As shown in Fig. 1, a custom manifold was designed to interface optical fibres with DMF devices for in-plane analysis (the .stl file for the design is included in the ESM). The manifold was designed to accommodate commercial finger-tight threaded optical connectors, which allow for rapid and reproducible insertion, alignment and adjustment of optical fibre positioning in DMF devices. Fibres can be removed when not needed to save device space and easily reinserted when necessary. Further, the system was designed such that the droplets do not touch the fibres (in contrast to the system reported previously [28]) to avoid potential problems with adsorption onto the fibres. In most of the experiments described here, two fibres were used—a source fibre that was connected to a mini spectrometer (USB4000, Ocean Optics) and a collection fibre that was connected to a miniature pulsed Xenon lamp (PX-2, Ocean Optics). These two instruments (plus the manifold) occupy a combined space of just 140 mm × 105 mm × 75 mm (about the size of a box of tissues). The scheme was designed to be flexible—in the future, it might be used with additional fibres for multiplexing or larger or smaller components as required by the application.

An absorbance spectrum of a droplet containing a model analyte (thymol blue) collected using the new system is shown in Fig. 2a—note the characteristic peak at ~600 nm. An 18-

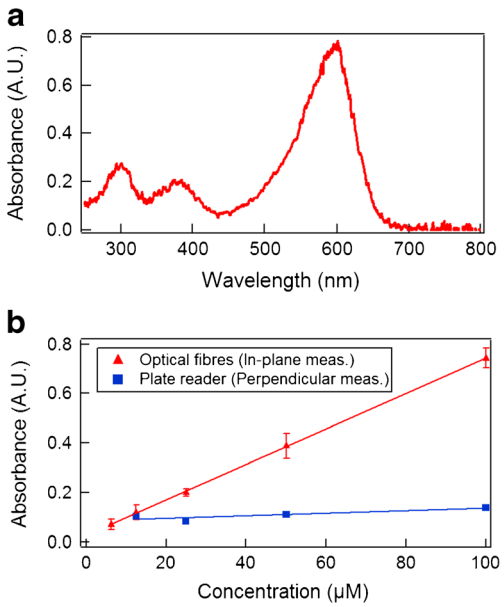

Fig. 2 Absorbance measurements in droplets. (**a**) Absorbance spectrum of thymol blue (pH 10) acquired on-chip using the in-plane analysis method. (**b**) Absorbance calibration curves (λ=600 nm) from an on-chip serial dilution of thymol blue droplets measured perpendicularly (*blue squares*) with a well plate reader and in-plane (*red triangles*) using the new optical fibre technique. *Error bars* represent ±one standard deviation, *n*=4

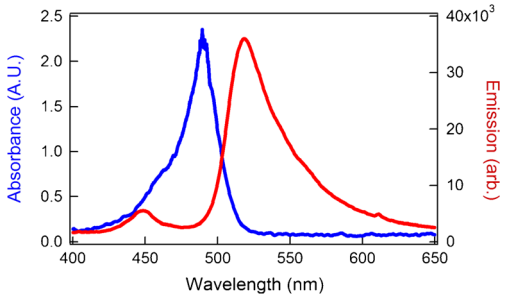

Fig. 3 Multi-modal analysis. Absorbance (*blue*) and fluorescence emission (*red*) spectra of a droplet of fluorescein (10 μM, pH 10.1) acquired using the in-plane DMF optical fibre system

step digital microfluidic protocol was developed to generate a dilution series of six different concentrations of thymol blue. As shown in Fig. 2b, the process was repeated, and absorbance values at 600 nm (red triangles) had excellent linearity (R^2=0.9998) over more than an order of magnitude. For comparison, a similar process was developed to evaluate the same concentrations using a conventional, perpendicular alignment (blue squares). As shown, the calibration data generated using the vertical alignment has poorer linearity (R^2= 0.7694) and is ~14× less sensitive (vertical measurement slope=0.0005; in-plane measurement slope=0.0072). This difference in sensitivity is approximately double the difference expected from the path length difference (~7-fold for 270 μm vs. 2 mm); we attribute the additional enhancement to a 'liquid lens' effect (described below).

We note that the precision observed for the new method (in which coefficients of variation, CVs, range from 5 to 29 %) is poorer than that of the vertical technique (in which CVs range from 2 to 8 %). The increased variance observed for the new method is likely caused by variations in volumes associated with dispensing (from reservoirs) and splitting (from mixtures of analyte and diluent). This variance is compounded for the in-plane technique, affecting both the concentration in the droplets and

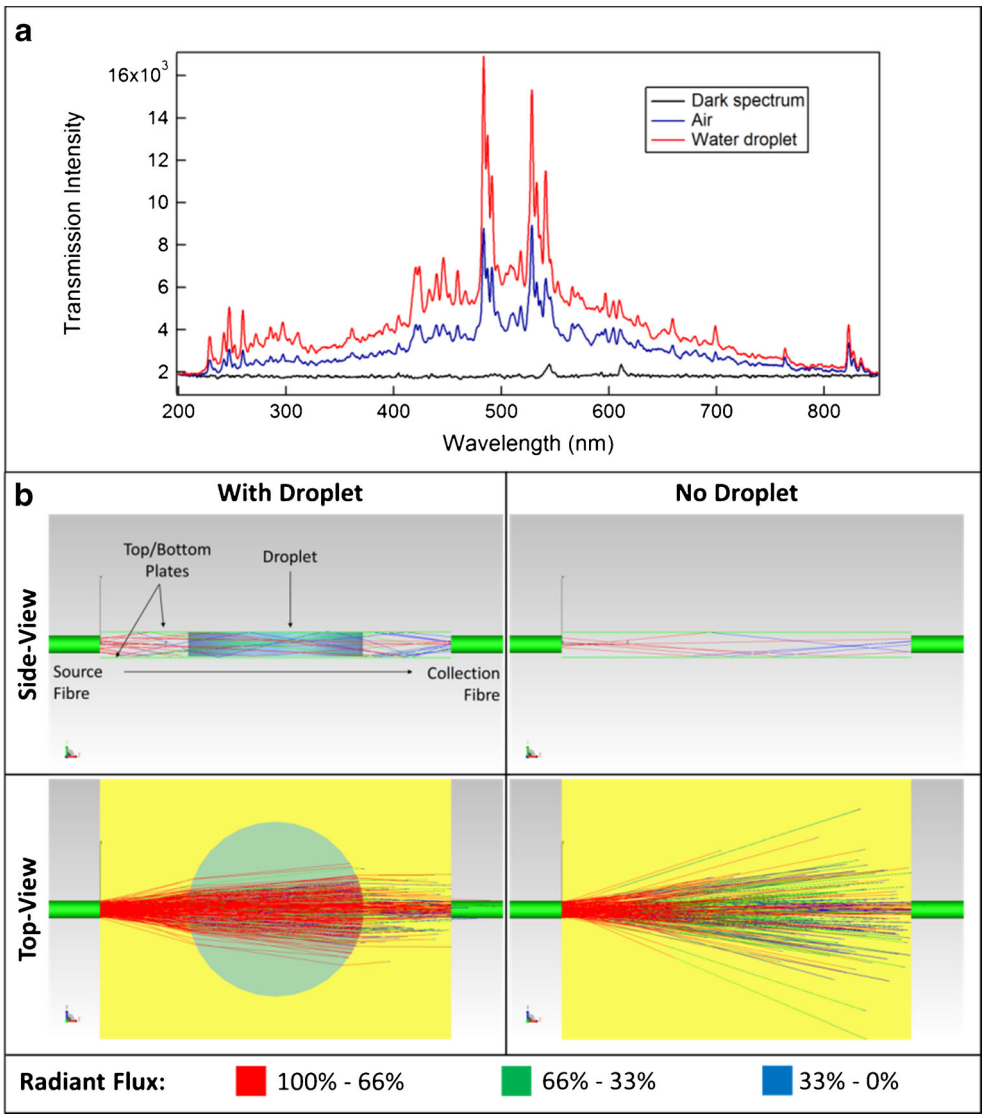

Fig. 4 Liquid lens effect. (**a**) Transmission spectra of Xenon light source collected with a water droplet (*red*) and without a droplet (*blue*) positioned between the source and collection fibres on the device. A third spectrum in *black* shows the spectrum collected when the Xenon source is off and a water droplet is not present. (**b**) Ray tracing simulations of light passing between source and collection fibres with and without a water droplet positioned in the gap. In the *side view* (*top*), only rays reaching the collection fibre are shown, and internal reflection within the droplet is visible. In the *top view* (*bottom*), all rays are shown, and increased transmission from refraction is evident. Each ray is colour coded by intensity, with *red*, *green* and *blue* rays possessing 66–100, 33–66 or 0–33 %, respectively

the path length of the samples. We propose that in the future, this problem may be mitigated by using feedback-controlled electronic control over droplet position, which enables more precise dispensing and splitting [33, 34] (in the experiments reported here, timing and duration were controlled manually). Regardless, the precision described here was sufficient to explore the feasibility of this technique to demonstrate proof of concept.

An additional comparison was made between the new technique and the popular NanoDrop (ThermoScientific) microvolume spectrometer. In the NanoDrop, a single 0.5–2.0-μL droplet of analyte is suspended vertically between a light source and a collector optic with a path length determined by volume. An identical dilution series of thymol blue was prepared off-chip and analysed using a NanoDrop, and a regression curve (R^2=0.9989, CVs 2.7–13 %) fitted to that data revealed that the calibration sensitivity (slope=0.0027) is ~2.5× lower than that of the new method reported here. Further, because some NanoDrops are designed for multimodal operation (enabling fluorescence spectroscopy measurements in addition to absorbance spectroscopy), the new DMF optical fibre interface was also tested for feasibility of multimodal operation (Fig. 3). A single analyte droplet was interrogated in both absorbance and fluorescence modes, requiring only minimal reconfiguration of the optical fibre detection system; to switch to fluorescence mode, the Xenon lamp is disabled and a perpendicular excitation source is enabled. We propose that the combination of high-performance multi-modal optical analysis with complex sample processing regimens (e.g. an 18-step dilution series) positions the new method as a useful new tool for microscale spectrophotometry.

Droplet shape effects

The curved interface adopted by a liquid droplet suspended in an immiscible medium makes it particularly interesting to characterise with optical spectroscopy. For example, scientists using an alternative microfluidic motif in which emulsions of aqueous droplets in an oil carrier fluid are pumped through enclosed channels have reported droplet dye lasers [35] and whispering gallery mode resonators [36]. We hypothesised that the circular droplet shape might have related effects in the methods reported here, in which circular 'pancake-shaped' droplets are suspended in a matrix of air. Further, we anticipated that reflection from the chromium driving electrodes used in DMF (exploited in the recent report of a DMF-driven dye laser [37]) would provide additional enhancement for the new method.

To test potential 'liquid lens' effects of the system evaluated here, transmission spectra for the Xenon lamp optical source (Fig. 4a) were collected with (red) and without (blue) a unit droplet in the space between the source and collector fibres. As shown, the presence of a droplet in the gap results in a signal enhancement of 1.9±0.3-fold (signal±standard deviation, integrated over 2,785 points in a spectrum from 250 to 800 nm) relative to the case with no droplet in the gap. This enhancement was probed with optical ray tracing simulations (Fig. 4b), revealing a potential focusing effect caused by refraction at the curved water–air interface (most obvious in the top view) and a potential total internal reflection effect (most obvious in the side view). In sum, the simulation predicts a 2.4-fold 'liquid lens' enhancement, which is similar to the experimental observation of a 1.9-fold enhancement

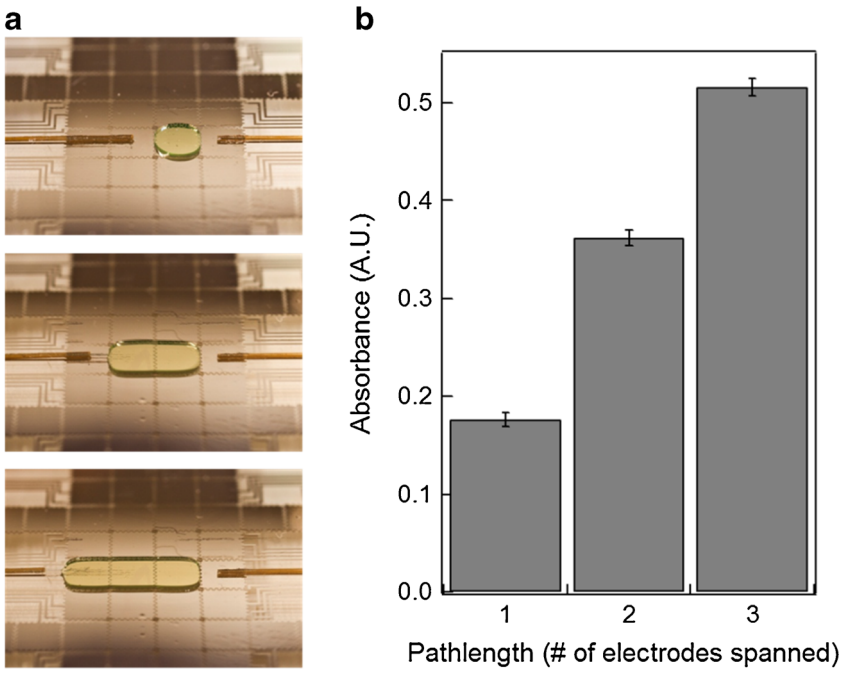

Fig. 5 Variable path length measurements. (**a**) Pictures of droplets spanning one (*top*), two (*middle*) and three (*bottom*) electrodes. (**b**) Graph of absorbance (λ=488 nm) in droplets of 10 μM fluorescein in 20 mM borate buffer (pH 10.1) as a function of droplet width (reported as no. of electrodes spanned). *Error bars* represent one standard deviation, *n*=4

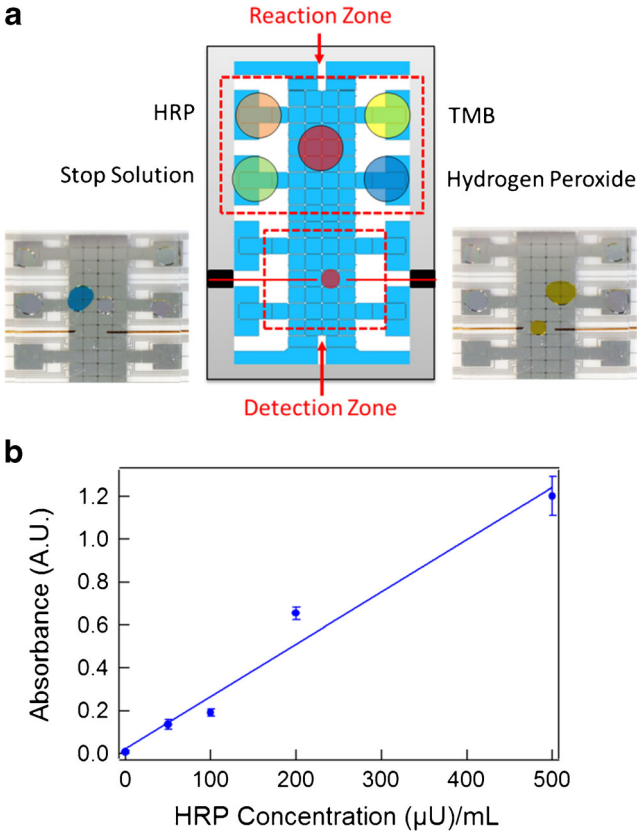

Fig. 6 Optical fibre measurement system for on-chip enzymatic colorimetric assay. (**a**) Device schematic and pictures showing a droplet of stop solution being brought to a mixture of HRP, TMB and H_2O_2 solutions in the extraction zone and the final mixture in the detection zone. Dyes were added to enhance colour for photos. (**b**) Absorbance calibration curve for a horse radish peroxidase (HRP) assay performed on-chip using the new optical fibre technique. Substrates were hydrogen peroxide and 3,3′,5,5′-tetramethylbenzidine (λ=460 nm). LOD=4.5 μU/mL. *Error bars* represent ±one standard deviation, n=4

(Fig. 4a). The difference between the experimental and predicted values may be caused by the simplifying assumptions made in designing the model, such as treating the chromium layer as a perfect reflector and modelling all surfaces as being perfectly smooth. In the future, more tests and a more accurate model may be designed to probe this phenomenon further.

An additional droplet-geometry effect that is unique to digital microfluidics is the capacity to evaluate samples of varying sizes. For example, by merging an initial unit droplet with zero, one or two additional droplets, the path length can be rapidly switched between 1×, 2× or 3× aliquots. The optical fibre interface was designed to enable flexible alignment and transitions; for example, the analysis schemes for 1×, 2× and 3× aliquots shown in Fig. 5a were formed and switched in seconds. As expected, the increasing path lengths allow for greater sensitivity (Fig. 5b), in effect enabling a variable dynamic range for analysis. Note that this is quite unique relative to any other system that we are aware of (e.g. that the one in-plane DMF optical analysis system reported previously [28] has permanent path length that cannot be adjusted) and represents a feature that may be useful in the detection of trace analytes in which maximum sensitivity must be achieved.

Applications

Commercial standalone detectors such as the NanoDrop are commonplace; in contrast, the new system described here is unique in integrating high-performance optical detection with multi-step reactions and heterogeneous processing. Two applications were explored to illustrate this point. For the first application, we chose to evaluate an enzymatic colorimetric assay in which HRP catalyses the formation of a yellow-coloured product from a colourless substrate (TMB). In the experiments and results reported here, HRP assays were performed in the reaction zone of the DMF device, and the product droplets were then analysed using the new technique (Fig. 6a). Absorbance measurements of the products of the

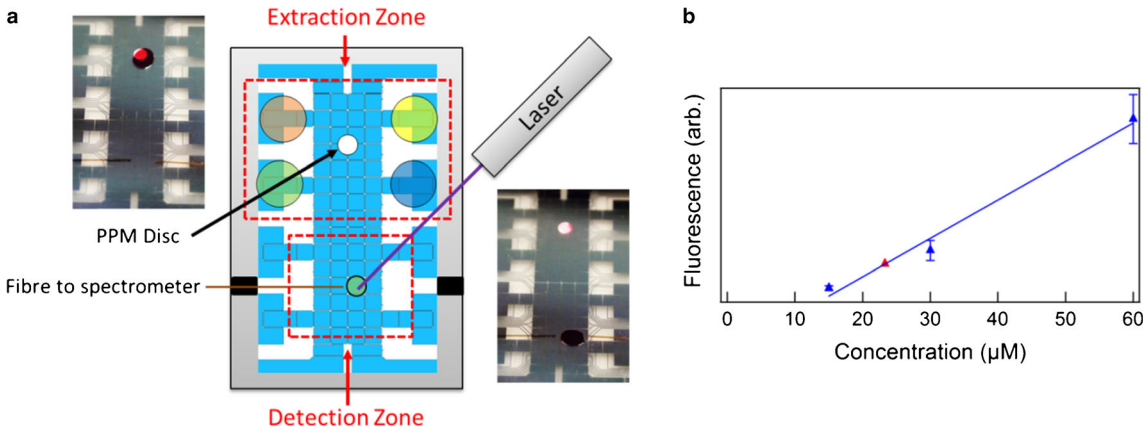

Fig. 7 Optical fibre system for measurement for DMF-SPE. (**a**) Device schematic and pictures showing delivery of analyte to porous polymer monolith disc in the extraction zone and interrogation of eluate droplet in the detection zone. (Note: in the pictures, the droplets contain red dye to improve visibility). (**b**) Fluorescence calibration curve for fluorescein (*blue triangles*) with sample eluate point (*red triangle*). Linear regression analysis (R^2=0.9856) of calibration data yields an eluate concentration of 23.3±2.3 μM. *Error bars* represent ±one standard deviation (n=3)

series of HRP standards and subsequent linear fit of the data (R^2=0.9707, CV 4–17 %). This performance is comparable to that of a chemiluminescent measurement technique reported for similarly sized droplets with signal collected perpendicularly [38].

As a second model application, the new system was used to implement a solid-phase extraction (SPE) procedure in which analytes are absorbed to and then eluted from C12-functionalized PPM discs [31]. As illustrated in Fig. 7a, SPE was performed in the reaction zone of a DMF device, followed by analysis of fluorescence intensity using the in-plane optical fibres with no need for manual intervention. Using calibration data for fluorescence measurements (Fig. 7b), the concentration of fluorescein in the eluate was found to be 23.3 ±2.3 μM. The key advantage to this new integration of DMF-SPE with the optical fibre detection system is the ability to rapidly analyse eluates in-line without the need for manual intervention. This represents a substantial advance relative the DMF-SPE experiments reported previously [31], in which on-chip extraction was followed by device disassembly, eluate collection by pipette and analysis in an external plate reader. The savings in time in labour afforded by the new optical fibre absorbance and fluorescence detection system for DMF make it a valuable technique for use with DMF-SPE.

Conclusion

We have developed a novel optical fibre-based UV/Vis absorbance and fluorescence detection system for on-chip interrogation of droplets in digital microfluidic systems. Optical fibres are held by a custom manifold which allows straightforward adjustment of fibre spacing and position without compromising alignment. By measuring in-plane through the width of a droplet, longer path lengths, and hence greater absorbance sensitivity, can be achieved versus traditional vertical through-device measurements. We predict the optical fibre DMF detection system will be of great use for many digital microfluidic absorbance and fluorescence experiments involving microvolume samples.

Acknowledgments We thank Dr. Lorenzo Gutierrez and Dr. Jihye Kim for their assistance in preparing the 3D-printed manifold. J.M.M. thanks the Natural Sciences and Engineering Research Council of Canada (NSERC) and the Ontario Graduate Scholarship programme for scholarships. A.R.W. thanks the Canada Research Chair (CRC) Program for a CRC. We thank NSERC and Abbott Diagnostics for funding.

References

1. An J, Carmichael WW (1994) Toxicon 32:1495–1507
2. Lin R, Patrick Ritz G (1993) Org Geochem 20:695–706
3. Hansen TVO, Simonsen MK, Nielsen FC, Hundrup YA (2007) Cancer Epidemiol Biomarkers Prev 16:2072–2076
4. Llobera A, Demming S, Wilke R, Büttgenbach S (2007) Lab Chip 7:1560–1566
5. Mogensen KB, Kutter JP (2009) Electrophoresis 30(Suppl 1):S92–S100
6. Vila-Planas J, Fernández-Rosas E, Ibarlucea B, Demming S, Nogués C, Plaza JA, Domínguez C, Büttgenbach S, Llobera A (2011) Nat Protoc 6:1642–1655
7. Llobera A, Demming S, Joensson HN, Vila-Planas J, Andersson-Svahn H, Büttgenbach S (2010) Lab Chip 10:1987–1992
8. De Pedro S, Cadarso VJ, Muñoz-Berbel X, Plaza JA, Sort J, Brugger J, Büttgenbach S, Llobera A (2014) Sensors Actuators A Phys 215:30–35
9. Lee KS, Lee HLT, Ram RJ (2007) Lab Chip 7:1539–1545
10. Sheridan AK, Stewart G, Ur-Reyman H, Suyal N, Uttamchandani D (2009) IEEE Sensors J 9:1627–1632
11. Llobera A, Wilke R, Büttgenbach S (2004) Lab Chip 4:24–27
12. Mao X, Waldeisen JR, Juluri BK, Huang TJ (2007) Lab Chip 7:1303–1308
13. Lau AY, Lee LP, Chan JW (2008) Lab Chip 8:1116–1120
14. Zheng G, Lee SA, Yang S, Yang C (2010) Lab Chip 10:3125–3129
15. Yin D, Lunt EJ, Rudenko MI, Deamer DW, Hawkins AR, Schmidt H (2007) Lab Chip 7:1171–1175
16. Choi D, Kang T, Cho H, Choi Y, Lee LP (2009) Lab Chip 9:239–243
17. Loock H-P, Barnes JA, Gagliardi G, Li R, Oleschuk RD, Wächter H (2010) Can J Chem 88:401–410
18. Pollack MG, Fair RB, Shenderov AD (2000) Appl Phys Lett 77:1725–1726
19. Choi K, Ng AHC, Fobel R, Wheeler AR (2012) Annu Rev Anal Chem 5:413–440
20. Crassous J, Gabay C, Liogier G; Berge B (2004) In: Jiang W; Suzuki Y, (eds) Proceedings of SPIE - The International Society for Optical Engineering, vol. 5639, pp 143–148
21. Schultz P, Cumby B, Heikenfeld J (2012) Appl Opt 51:3744–3754
22. Reza SA, Riza NA (2009) Opt Commun 282:1298–1303
23. Au SH, Shih SCC, Wheeler AR (2011) Biomed Microdevices 13:41–50
24. Srinivasan V, Pamula VK, Fair RB (2004) Lab Chip 4:310–315
25. Wijethunga PAL, Nanayakkara YS, Kunchala P, Armstrong DW, Moon H (2011) Anal Chem 83:1658–1664
26. Dudus A, Blue R, Uttamchandani DI (2014) 2014 International Conference on Optical MEMS and Nanophotonics. IEEE 2014:123–124
27. Mach P, Krupenkin T, Yang S, Rogers JA (2002) Appl Phys Lett 81:202
28. Ceyssens F, Witters D, Van Grimbergen T, Knez K, Lammertyn J, Puers R (2013) Sensors Actuators B Chem 181:166–171
29. Ng AHC, Choi K, Luoma RP, Robinson JM, Wheeler AR (2012) Anal Chem 84:8805–8812
30. Eydelnant IA, Betty Li B, Wheeler AR (2014) Nat Commun 5:3355
31. Yang H, Mudrik JM, Jebrail MJ, Wheeler AR (2011) Anal Chem 83:3824–3830
32. Ro KWK, Lim K, Shim BBC, Hahn JJH (2005) Anal Chem 77:5160–5166
33. Fobel R, Fobel C, Wheeler AR (2013) Appl Phys Lett 102:193513
34. Liu Y, Banerjee A, Papautsky I (2014) Microfluid Nanofluid 17:295–303
35. Tang SKY, Li Z, Abate AR, Agresti JJ, Weitz DA, Psaltis D, Whitesides GM (2009) Lab Chip 9:2767–2771
36. Ta VD, Chen R, Sun HD (2013) Sci Rep 3:1362
37. Kuehne AJC, Gather MC, Eydelnant IA, Yun S-H, Weitz DA, Wheeler AR (2011) Lab Chip 11:3716–3719
38. Choi K, Ng AHC, Fobel R, Chang-Yen DA, Yarnell LE, Pearson EL, Oleksak CM, Fischer AT, Luoma RP, Robinson JM, Audet J, Wheeler AR (2013) Anal Chem 85:9638–9646